

Theory of topological quantum phase transitions in 3D noncentrosymmetric systems

Bohm-Jung Yang,¹ Mohammad Saeed Bahramy,¹ Ryotaro Arita,^{1,2} Hiroki Isobe,² and Naoto Nagaosa^{1,2,3}

¹*Correlated Electron Research Group (CERG), RIKEN Advanced Science Institute, Wako, Saitama 351-0198, Japan*

²*Department of Applied Physics, University of Tokyo, Tokyo 113-8656, Japan*

³*Cross-Correlated Material Research Group (CMRG), RIKEN Advanced Science Institute, Wako, Saitama 351-0198, Japan*

(Dated: July 27, 2012)

We have constructed a general theory for a new class of topological quantum phase transitions in 3D systems with broken inversion symmetry. Although the consideration of the system's codimension predicts the appearance of a stable metallic phase between the normal and topological insulators, when the band touching occurs along the direction with high crystalline symmetry, a direct topological phase transition between two insulators can occur. At the quantum critical point (QCP), the energy dispersion becomes quadratic along one direction while the dispersions along the other two orthogonal directions are linear, which manifests the zero chirality of the band touching point. Due to the anisotropic dispersion at QCP, various thermodynamic and transport properties show unusual temperature dependence and anisotropic behaviors.

PACS numbers:

The 3D topological insulator (TI) is a new state of matter in which the nontrivial topology of bulk electronic wave functions guarantees the existence of gapless states on the sample's boundary. [1, 2] Because of its topological nature, the surface gapless states are protected against small perturbations preserving the time-reversal symmetry as long as the bulk band gap remains finite. Therefore to change the bulk topological property, the band gap should be closed at some points in the Brillouin zone (BZ) via accidental band crossings. Recently, such a topological phase transition is realized in $\text{BiTi}(\text{S}_{1-x}\text{Se}_x)_2$ [3, 4], by modulating the spin-orbit interaction or the crystal lattice. In the systems with lattice inversion symmetry such as $\text{BiTi}(\text{S}_{1-x}\text{Se}_x)_2$, the topological quantum phase transition can be described by the (3+1) dimensional massive Dirac Hamiltonian in general. In this sense, the quantum phase transition of 3D TIs provides a new venue to study intriguing quantum critical behaviors of 3D particles with relativistic dispersion. [5–7]

On the other hand, for systems lacking inversion symmetry, our understanding of the topological quantum phase transition and corresponding quantum critical behavior is still incomplete. Based on the consideration of the codimension for an accidental band crossing, a stable metallic phase was predicted to appear between TI and normal insulator in 3D noncentrosymmetric systems. [8] The intervening metallic phase between two insulators, dubbed a Weyl semi-metal, has topological stability in the sense that there are several gapless points (Weyl points) with nonzero chiral charge at the Fermi level. [9] Therefore before every Weyl point is annihilated by colliding with another Weyl point with opposite chiral charge, the Weyl semi-metal should stably survive across the topological phase transition. In this respect, the recent discovery of a direct topological phase transition between two insulators in noncentrosymmetric compound BiTeI is an unexpected surprise. [10–12] At the QCP of BiTeI , instead of a Weyl semi-metal, several isolated band touching points with anisotropic dispersion appear mediating two insulating phases, which suggests the diversity of the possible phase dia-

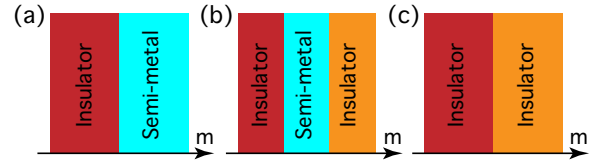


FIG. 1: (Color online) Generic phase diagrams, resulting from accidental band touching between conduction and valence bands in the 3D noncentrosymmetric systems. Three different types of phase diagrams are possible. Here, m indicates an external control parameter.

grams of noncentrosymmetric systems accessible via accidental band crossings.

In this paper, we propose generic phase diagrams for 3D noncentrosymmetric systems that can be achieved through accidental band crossings, as depicted in Fig. 1. The key ingredient to obtain Fig. 1 is the fact that the gap-closing point at QCP does not carry any topological quantum number, i.e., the chirality is zero. Therefore it can be either gapped out leading to another insulator (Fig. 1 (c)) or split into several Weyl points resulting in a Weyl semi-metal. In the latter case, depending on whether the trajectory, traversed by the gapless point, has a finite torsion or not, the Weyl semi-metal phase persists all the way (Fig. 1 (a)) or turns into another insulator (Fig. 1 (b)). In all three cases, at the QCP between two neighboring phases, the energy dispersion near a band touching point is highly anisotropic. Namely, the dispersion is linear along two orthogonal directions but is quadratic along the other third direction. This anisotropic band dispersion induces new power laws in the temperature dependence of various measurable quantities and anisotropic physical responses.

Phase transition through accidental band touching.— In systems with broken inversion symmetry, the accidental band touching between a conduction band and a valence band can be described by the following 2×2 Hamiltonian, $H(\mathbf{k}, m) = f_0(\mathbf{k}, m) + \sum_{i=1}^3 f_i(\mathbf{k}, m)\tau_i$, where $f_{0,1,2,3}$ are real functions and $\tau_{1,2,3}$ are Pauli matrices indicating the two bands. Here m describes a parameter, such as external pressure, which can

be tuned across the phase transition. In particular, we consider the following situation. For $m < m_c$, the system is fully gapped. An isolated band touching point occurs at the critical point $(\mathbf{k}, m) = (\mathbf{k}_c, m_c)$ where $f_{1,2,3}(\mathbf{k}_c, m_c) = 0$. Since f_0 does not affect the band touching, we neglect f_0 in the following discussion. Then the next question is what happens if m is increased further, i.e., when $m > m_c$. To examine the system's behavior near the phase transition point at (\mathbf{k}_c, m_c) , we derive the low energy Hamiltonian through an expansion in powers of $\mathbf{q} = \mathbf{k} - \mathbf{k}_c$ and $\Delta m = m - m_c$. Up to the linear order of \mathbf{q} and Δm , $\mathbf{f} = (f_1, f_2, f_3)^T$ (T stands for transpose) can be written as

$$\mathbf{f}(\mathbf{q}, \Delta m) = \hat{M}\mathbf{q} + \Delta m\mathbf{N}, \quad (1)$$

where $\hat{M}_{ij} = \frac{\partial f_i}{\partial q_j}|_{\mathbf{q}=\Delta m=0}$ and $N_i = \frac{\partial f_i}{\partial m}|_{\mathbf{q}=\Delta m=0}$. If the determinant of \hat{M} , i.e., $\text{Det}\hat{M}$ is nonzero, the gap-closing condition $\mathbf{f} = 0$ leads to $\mathbf{q} = -\hat{M}^{-1}\mathbf{N}\Delta m$, which means that the gapless point moves as Δm varies and persists even when $\Delta m < 0$ contradicting the initial assumption. Therefore $\text{Det}\hat{M}=0$ at the phase transition point. In fact, the sign of $\text{Det}\hat{M} = \varepsilon_{ijk}M_{1i}M_{2j}M_{3k}$ is the chirality (or chiral charge) of the gapless point at $\Delta m = 0$. Since the chirality is a topological number, when a band touching point has a nonzero chirality, it is stable against small external perturbations. However, when $\text{Det}\hat{M}=0$, it is not topologically protected. Therefore when an external parameter changes i.e., $\Delta m > 0$, the band touching point can either be gapped out leading to another insulating phase or be split into several gapless points with zero net chirality generating a stable metallic phase. When both of these possibilities are allowed, the insulating phase should be preferred since the gapped phase has lower energy.

To understand the nature of the ground state for $\Delta m > 0$, it is useful to rotate the momentum coordinate using a basis which manifests the zero chirality of the band touching point at $\Delta m = 0$. Since $\text{Det}\hat{M}=0$, \hat{M} has an eigenvector \mathbf{n}_1 with zero eigenvalue satisfying $\hat{M}\mathbf{n}_1 = 0$. We introduce two additional normalized vectors $\mathbf{n}_2, \mathbf{n}_3$, which can form an orthonormal basis $\{\mathbf{n}_1, \mathbf{n}_2, \mathbf{n}_3\}$, and construct a matrix $\hat{W} = (\mathbf{n}_1, \mathbf{n}_2, \mathbf{n}_3)$. With the rotated coordinate $\mathbf{p} = \hat{W}^{-1}\mathbf{q}$, Eq. (1) can be written as, $\mathbf{f}(\mathbf{p}, \Delta m) = \mathbf{u}_2 p_2 + \mathbf{u}_3 p_3 + \Delta m\mathbf{N}$, where $\mathbf{u}_{2,3} = \hat{M}\mathbf{n}_{2,3}$. It is worth to note that p_1 linear term does not appear in \mathbf{f} due to the fact that $\hat{M}\mathbf{n}_1 = 0$. If the band touching occurs at an arbitrary point with no symmetry constraint in the momentum space, the leading contribution of p_1 dependent term starts from the quadratic order, which leads to the minimal effective Hamiltonian $H(\mathbf{p}, \Delta m) = \sum_{i=1}^3 f_i(\mathbf{p}, \Delta m)\tau_i$ in which

$$\mathbf{f}(\mathbf{p}, \Delta m) = \mathbf{u}_2 p_2 + \mathbf{u}_3 p_3 + \mathbf{u}_4 p_1^2 + \Delta m\mathbf{N}. \quad (2)$$

However, if the band touching points are under some symmetry constraint, the contributions of other quadratic terms $p_i p_j$ should be included to construct the correct low energy Hamiltonian.

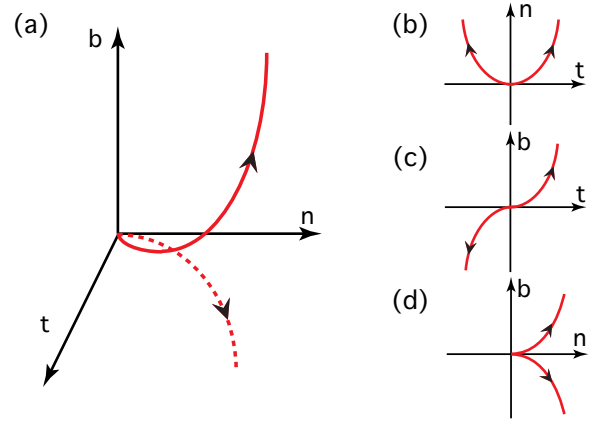


FIG. 2: (Color online) (a) Typical shape of a curve with nonzero curvature and torsion in 3D space. 2D Projections of the curve onto (b) (t, n) plane, (c) (t, b) plane, (d) (n, b) plane. Here two arrows describe the flowing directions of two band touching points which are generated from the QCP at the origin.

Conditions to obtain a semi-metal.— Now let us discuss about the ground states for $\Delta m > 0$. At first we consider the case of a stable (topological) metallic phase which can be obtained by splitting the band touching point at $\Delta m = 0$ into two gapless points with opposite chiralities. Since there are 4 parameters ($p_{1,2,3}$ and Δm) although only 3 conditions of $f_{1,2,3} = 0$ are required to be satisfied to achieve a gapless phase, there is a line of gapless points in the $(\mathbf{p}, \Delta m)$ space in general. Regarding $t \equiv \Delta m$ as a parameter, the trajectories of the two gapless points form a curve $\mathbf{p}^*(t) = (x^*(t), y^*(t), z^*(t))$ in 3D momentum space. Then the ground state phase diagram can be determined by the shape of the curve in the 3D space. Namely, if the trajectory makes an open curve, the semi-metal phase is expected to persist for $\Delta m > 0$ corresponding to the phase diagram in Fig. 1 (a). On the other hand, if the curve forms a closed loop, there is another transition from the semi-metal to an insulator leading to the phase diagram in Fig. 1 (b).

A convenient way to describe a curve $C(t) = (x(t), y(t), z(t))$ is to use an orthogonal coordinate system $(\mathbf{t}, \mathbf{n}, \mathbf{b})$ where $\mathbf{t}, \mathbf{n}, \mathbf{b} = \mathbf{t} \times \mathbf{n}$ are the tangential, normal, and binormal vectors, respectively. The shape of a curve C near the initial point at $t = 0$ can be determined once the curvature κ_C and the torsion τ_C are specified at $t = 0$. [13] Here κ_C measures the rate at which the tangential vector changes and τ_C measures the rate at which the curve C deviates from being a planar curve lying on the (\mathbf{t}, \mathbf{n}) space. The relation between the shape of a curve and its curvature and torsion can be understood by considering two dimensional projections of the curve on the planes in which two vectors among $\{\mathbf{t}, \mathbf{n}, \mathbf{b}\}$ are adopted as a basis. After choosing a coordinate properly, the projections of the curve C are described by $y = \frac{\kappa_C}{2}x^2$, $z = \frac{\kappa_C\tau_C}{6}x^3$, and $z^2 = \frac{2}{9}\frac{\tau_C^2}{\kappa_C}y^3$, which are lying on (\mathbf{t}, \mathbf{n}) , (\mathbf{t}, \mathbf{b}) , and (\mathbf{n}, \mathbf{b}) planes, respectively. A typical example of a curve in 3D and its 2D projections are shown in Fig. 2.

Considering the projections of the curve on (\mathbf{t}, \mathbf{b}) and (\mathbf{n}, \mathbf{b}) planes, shown in Fig. 2 (c) and (d), respectively, we can see that the trajectory cannot form a closed curve under smooth variations as long as the torsion τ_C is nonzero. The semi-metallic phase should persist in this case. (Fig. 1 (a)) An example where gapless points form a curve with nonzero τ_C is shown in the supplementary material. [14] On the other hand when $\tau_C = 0$, the curve moves only on the 2D space spanned by (\mathbf{t}, \mathbf{n}) . The trajectory of the curve on (\mathbf{t}, \mathbf{n}) plane shown in Fig. 2 (b) can make a closed loop as long as the curvature κ_C is finite. In this case, it is expected that there can be another phase transition to an insulator through pair annihilations of band touching points. (Fig. 1 (b)) Therefore the fate of the semi-metallic phase is determined by the torsion τ_C of the curve corresponding to the trajectory of band touching points.

Conditions to obtain an insulator.— Now we turn to the conditions to have a gapped phase for $\Delta m > 0$ corresponding to Fig. 1 (c). Since the system is gapped for $\Delta m \neq 0$, the conduction (valence) band should have a well-defined dispersion minimum (maximum) near $\mathbf{p} = 0$, which can allow a band touching locally in momentum space at $\Delta m = 0$. Considering the minimal 2×2 Hamiltonian with $f_{1,2,3}(\mathbf{p}, \Delta m)$ in Eq. (2), the energy eigenvalue of the conduction band is given by $E_c(\mathbf{p}, \Delta m) = \sqrt{\sum_{i=1,2,3} f_i^2(\mathbf{p}, \Delta m)}$. The condition to have an extremum for small $\Delta m \neq 0$ leads to the following three equations $g_i = \partial E_c(\mathbf{p}, \Delta m) / \partial p_i = 0$ ($i = 1, 2, 3$). After solving the 3 coupled equations, the general solution for the location of the dispersion minimum is obtained as $\mathbf{p}^{\min} = (0, A\Delta m, B\Delta m)$ where A, B are some constants. It is important to notice that the conduction (valence) band minimum (maximum) should move along the line that satisfies $p_1 = 0$ and $p_2 = \frac{A}{B}p_3$ for both $\Delta m < 0$ and $\Delta m > 0$ across the phase transition, which can be achievable generally when the system has high crystalline symmetry along the line. Moreover, due to time reversal invariance, the band structure at momenta $\pm \mathbf{k}$ should be equivalent. Therefore the extrema in band dispersions of the gapped phases should move along the line with high crystalline symmetry which passes through a time reversal invariant momentum at the center.

To understand the shape of the band near the dispersion minimum, we compute the Hessian matrix $\hat{H}_{ij}^{\min} = \frac{\partial^2 E_c}{\partial p_i \partial p_j}$, which has a block diagonal form with $\hat{H}_{12}^{\min} = \hat{H}_{13}^{\min} = 0$ at $\mathbf{p} = \mathbf{p}^{\min}$. The other nonzero components of \hat{H}^{\min} satisfies

$$\hat{H}_{11}^{\min} = c_{11}\Delta m, \quad \text{Det} \begin{pmatrix} H_{22}^{\min} & H_{23}^{\min} \\ H_{32}^{\min} & H_{33}^{\min} \end{pmatrix} > 0,$$

where c_{11} is a constant. Interestingly, \hat{H}_{11}^{\min} changes the sign across the phase transition because it is linearly proportional to Δm . For $c_{11} < 0$ ($c_{11} > 0$), the conduction band has a dispersion minimum in all three directions for $\Delta m < 0$ ($\Delta m > 0$) while it has a saddle point with a negative curvature along the p_1 direction for $\Delta m > 0$ ($\Delta m < 0$). Therefore when there is a direct phase transition between two insulators, one of them has to possess a saddle point at the bottom (top)

of the conduction (valence) band along the p_1 direction where the energy dispersion is quadratic at QCP.

Topological phase transition— A direct phase transition between two insulators via accidental band touching can accompany the change of bulk topological properties. In 3D time-reversal invariant systems, band insulators can be classified by Z_2 topological numbers ν_i ($i = 0, 1, 2, 3$). [1, 15, 16] In the BZ, there are 3 pairs of parallel planes, in which $\mathbf{k} \cdot \mathbf{a}_i = 0$ or π . ($i = 1, 2, 3$) Here $\mathbf{a}_{1,2,3}$ are primitive lattice vectors. Since each of the planes satisfies the time reversal symmetry $TH(\mathbf{k})T^{-1} = H(-\mathbf{k})$ with time reversal operator T , a 2D Z_2 invariant α_i^0 (α_i^π) can be assigned to each plane satisfying $\mathbf{k} \cdot \mathbf{a}_i = 0$ ($\mathbf{k} \cdot \mathbf{a}_i = \pi$). Since $\alpha_1^0 + \alpha_1^\pi = \alpha_2^0 + \alpha_2^\pi = \alpha_3^0 + \alpha_3^\pi$, only four 2D invariants are independent and determine the Z_2 invariants of the 3D system in the following way, $(\nu_0, \nu_1, \nu_2, \nu_3) = (\alpha_1^0 + \alpha_1^\pi, \alpha_1^\pi, \alpha_2^\pi, \alpha_3^\pi)$. The strong invariant ν_0 distinguishes a TI ($\nu_0 = 1$) and a band insulator ($\nu_0 = 0$). Since $\nu_0 = \alpha_i^0 + \alpha_i^\pi$ for any $i = 1, 2, 3$, if one of 2D Z_2 invariants changes by 1 through the accidental band touching, a topological phase transition occurs.

In a 2D BZ with time-reversal invariance, the Z_2 invariant α is given by the Chern number (modulo 2), which is the integral of the Berry curvature over the half of the BZ (with additional contraction procedures). [15] Therefore if the band touching between the valence and conduction bands, which changes the Chern number of each band by ± 1 per single touching [17], occurs odd number of times in a half of the BZ, α changes by 1 leading to the 3D topological phase transition. Therefore when the direct phase transition between two insulators happens, if the line with high crystalline symmetry embracing QCPs is lying on the 2D planes with time-reversal invariance and the number of such lines is odd, the topological property of the two insulators should be different.

Application to the topological quantum phase transition of pressured BiTeI.— Recently, it is theoretically demonstrated that when an external pressure P is applied to BiTeI, a direct phase transition from a normal insulator to a TI occurs mediated by accidental band touching points at the critical pressure P_c [12]. The origin of the direct phase transition in BiTeI can be understood based on the general considerations developed in previous discussions. The key ingredient is the fact that the band touching occurs along the line with high symmetry ($A-H$ line) in $k_z = \pi$ plane (BZ of BiTeI is shown in Fig. 1 of [12]). Because of the C_{3v} point group symmetry, the conduction (valence) band with the Rashba-type spin-orbit coupling develops a dispersion minimum (maximum) along this line for any pressure across the accidental band crossing, which satisfies the necessary condition to achieve the direct transition. Moreover, since the high symmetry line is on the $k_z = \pi$ plane satisfying the time-reversal invariance, the band touching can induce the topological phase transition. In Fig. 3, we plot the evolution of the band dispersion across the topological phase transition near one of band touching points using the band structure obtained by first principle calculations. [18] At the QCP, the band dispersion is quadratic along one direction (p_1) and linear along the other two orthogonal directions (p_2

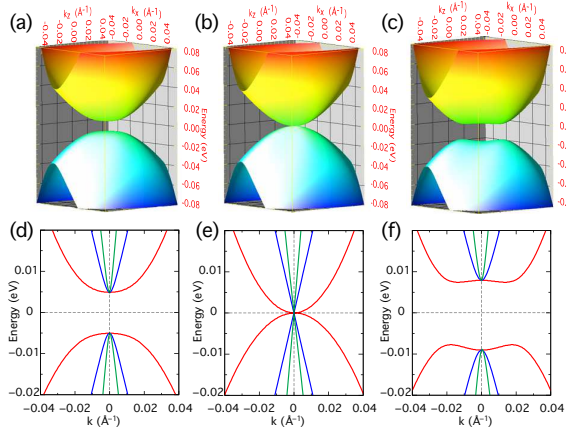


FIG. 3: (Color online) Evolution of the band structure, obtained from first-principle calculations, across the topological phase transition in BiTeI. Energy dispersion of the conduction/valence bands near one of the band touching point in (p_1, p_2) plane, which is normal to the high symmetry line embracing QCPs, is shown for (a) $P < P_c$, (b) $P = P_c$, (c) $P > P_c$, respectively. Energy dispersions along the p_1 (red), p_2 (green), p_3 (blue) directions are shown for (d) $P < P_c$, (e) $P = P_c$, and (f) $P > P_c$, respectively.

	$D(\varepsilon)$	$C_V(T)$	$\kappa(T)$	$\chi_D(T)$	$\sigma_{DC}(T)$
Weyl semi-metal	ε^2	T^3	T^2	$\ln T$	T
At the QCP	$\varepsilon^{3/2}$	$T^{5/2}$	$T^{3/2}$	$T^{-1/2}$	$T^{1/2}$

TABLE I: Summary of the leading temperature (or energy) dependence of various physical quantities for a 3D Weyl semi-metal and at the QCP. $D(\varepsilon)$, C_V , κ , χ_D , σ_{DC} are density of states, specific heat, compressibility, diamagnetic susceptibility, and the DC conductivity, respectively. For both the 3D Weyl semi-metal and at the QCP, we set the chemical potential to be at the band touching point. To compute $\sigma_{DC}(T)$, we have used the T-linear scattering rate due to Coulomb interaction, which is suitable for quantum critical systems.

and p_3). Moreover, across the QCP, the band dispersion of the insulating phase for $P > P_c$ possesses a saddle point, which proves the direct topological phase transition.

Thermodynamic properties at QCP.— The most important characteristics of the QCP is the anisotropic dispersion, which leads to the following minimal Hamiltonian at the QCP,

$$H_{\text{QCP}}(\mathbf{p}) = Ap_1^2\tau_1 + vp_2\tau_2 + vp_3\tau_3. \quad (3)$$

where v is the velocity and A is the inverse mass along the p_1 direction. The anisotropic dispersion gives rise to a peculiar power law in the density of states such as $D(\varepsilon) \propto \varepsilon^{3/2}$, which is quite distinct from that for a 3D Weyl semi-metal ($D(\varepsilon) \propto \varepsilon^2$) or a 3D normal metal with quadratic dispersion ($D(\varepsilon) \propto \varepsilon^{1/2}$). This distinct power law of $D(\varepsilon)$ directly leads to new exponents in the temperature dependence of various thermodynamic quantities such as the specific heat (C_V) and compressibility (κ) as summarized in Table I. The diamagnetic susceptibility χ_D also shows an unexpected singular behavior. We have computed χ_D using the Fukuyama formula for the orbital susceptibility $\chi_D =$

$\frac{e^2}{c^2} \frac{T}{V} \sum_{n,\mathbf{p}} \text{Tr}[G\gamma_a G\gamma_b G\gamma_a G\gamma_b]$. [19] Here $\gamma_a \equiv \frac{\partial H_{\text{QCP}}}{\partial p_a}$ and a, b are two orthogonal directions perpendicular to the applied magnetic field. For the Hamiltonian in Eq. (3), χ_D is given by $\chi_D(\theta) = \cos^2 \theta \chi_1 + \sin^2 \theta \chi_2$, in which $\chi_1 \approx C_1 T^{-1/2}$ and $\chi_2 \approx \chi_2^0 + C_2 T^{1/2}$ with $\chi_2^0, C_{1,2}$ constants. Here θ is the angle between the external magnetic field and p_1 direction. Therefore χ_D shows unusual singular temperature dependence in low temperature given by $\chi_D \sim T^{-1/2}$ irrespective of magnetic field directions.

Anisotropic DC conductivity.— The anisotropic dispersion at QCP also induces anisotropic temperature dependence of the DC conductivities. Assuming momentum independence of the scattering rate $\tau(\omega)$, a straightforward calculation of the conductivity tensor using Kubo formula gives rise to the following expression of the DC conductivities,

$$\begin{aligned} \sigma_{11}(T) &= \frac{2e^2\sqrt{A}}{7\pi^2v^2} \int d\omega |\omega|^{5/2} \left(-\frac{\partial f}{\partial \omega} \right) \tau(\omega), \\ \sigma_{22,33}(T) &= \frac{9e^2}{20\pi^2\sqrt{A}} \int d\omega |\omega|^{3/2} \left(-\frac{\partial f}{\partial \omega} \right) \tau(\omega), \end{aligned} \quad (4)$$

When the Coulomb scattering is the dominant scattering mechanism, we can take $\frac{1}{\tau} = \alpha^2 T$ with $\alpha = \frac{e^2}{4\pi\varepsilon v}$ the typical scattering rate of quantum critical systems, taking into account of the fact that the low temperature transport is dominated by the linear dispersion. In this case, the temperature dependence of the DC conductivity is given by $\sigma_{11}(T) \propto T^{3/2}$ and $\sigma_{22,33}(T) \propto T^{1/2}$. On the other hand, when the scattering due to random potentials dominates the transport, using Born approximation, the leading contribution to the scattering rate can be obtained by $\frac{1}{\tau(\omega)} \approx 2\pi\gamma_0 D(\omega)$ with $\gamma_0 = \frac{n_i V_0^2}{2}$. [20] Here V_0 is the impurity scattering potential, n_i is the impurity density. Then using Eq. (4), we obtain $\sigma_{33}(T) = \frac{9e^2 v^2}{20\pi\gamma_0}$, $\sigma_{11}(T) = \frac{2e^2 A}{7\pi\gamma_0} (2 \ln 2) T$, which also shows the anisotropic T dependence. [21] In fact, Eq. (4) implies that, as long as the scattering rate does not show any momentum dependence, $\sigma_{33}(T)/\sigma_{11}(T)$ shows unusual temperature dependence, independent of the scattering mechanism such as $\frac{\sigma_{33}(T)}{\sigma_{11}(T)} = C_0 \frac{A}{v^2} T$ where $C_0 \approx 1.8$.

Stability of QCP.— Finally, let us discuss about the stability of the anisotropic QCP in Eq. (3) under the influence of disorder and long-ranged Coulomb interaction. The effective action of the QCP including both random disorder potential and $1/r$ Coulomb interaction can be written as

$$\begin{aligned} S &= \int dt d^3x [\psi^\dagger (i\partial_t + A\partial_1^2\tau_1 + \sum_{j=2,3} iv\partial_j\tau_j)\psi + V_i\psi^\dagger M_i\psi] \\ &+ \int dt d^3x d^3x' (\psi^\dagger\psi)_{x,t} \frac{g^2}{2|\mathbf{x}-\mathbf{x}'|} (\psi^\dagger\psi)_{x',t}. \end{aligned} \quad (5)$$

where $V_i(\mathbf{x})$ is a random potential coupled to fermion field $\psi(\mathbf{x})$ via a matrix M_i . $g^2 = e^2/\varepsilon$ where e and ε are the electric charge and dielectric constant, respectively. We take a random disorder potential with Gaussian invariance whose impurity average satisfies $\langle V_i(\mathbf{x})V_j(\mathbf{x}') \rangle = \Delta_{ij}\delta^{(3)}(\mathbf{x}-\mathbf{x}')$. The

key characteristics of the Gaussian fixed point in Eq. (3) is the invariance of the Hamiltonian under the anisotropic scaling of spatial coordinates, i.e., $\tilde{x}_1 = x_1/b^{1/2}$, $\tilde{x}_{2,3} = x_{2,3}/b$ accompanied by $\tilde{t} = t/b$ where the tilde indicates the new scaled coordinates. Under this scale transformation, Δ_{ij} transforms as $\tilde{\Delta}_{ij} = b^{-1/2}\Delta_{ij}$ showing that the disorder is an irrelevant perturbation. Similarly, it is straightforward to show that $\tilde{g}^2 = b^{-1/2}g^2$. Therefore both the random disorder potential and Coulomb interaction are irrelevant perturbations at the Gaussian fixed point. The same conclusion can be obtained even when we consider a generalized scaling transformation, i.e., $\tilde{t} = t/b^z$, $\tilde{x}_1 = x_1/b^{z_1}$, and $\tilde{x}_{2,3} = x_{2,3}/b$ within one-loop perturbative renormalization group calculation. [14] Therefore the unusual power laws in various thermodynamic and transport properties, which are predicted based on the free particle Hamiltonian in Eq. (3) should persist even under the influence of the disorder and Coulomb interaction.

This work is supported by the Japan Society for the Promotion of Science (JSPS) through the ‘‘Funding Program for World-Leading Innovative R&D on Science and Technology (FIRST Program)’’.

-
- [1] L. Fu, C. L. Kane, E. J. Mele, Phys. Rev. Lett. **98**, 106803 (2007).
 [2] X. -L. Qi, T. L. Hughes and S. -C. Zhang, Phys. Rev. B **78**, 195424 (2008).
 [3] S. -Y. Xu et al., Science **332**, 560 (2011).
 [4] T. Sato et al., Nat. Phys. **7**, 840 (2011).
 [5] P. Goswami and S. Chakravarty, Phys. Rev. Lett. **107**, 196803 (2011).
 [6] H. Isobe and N. Nagaosa, arXiv: 1205.2427.
 [7] P. Hosur, S. A. Parameswaran, and A. Vishwanath, Phys. Rev. Lett. **108**, 046602 (2012).
 [8] S. Murakami and S. -i. Kuga, Phys. Rev. B **78**, 165313 (2008); S. Murakami, New J. Phys. **9**, 356 (2007).
 [9] X. Wan, A. M. Turner, A. Vishwanath, and S. Y. Savrasov, Phys. Rev. B **83** 205101 (2011).
 [10] K. Ishizaka et al., Nat. Mater. **10** 521 (2011).
 [11] M. S. Bahramy, R. Arita, and N. Nagaosa, Phys. Rev. B **84** 041202(R) (2011).
 [12] M. S. Bahramy, B. -J. Yang, R. Arita, and N. Nagaosa, Nat. Commun. **3** 679 (2012).
 [13] M. Spivak, Differential Geometry vol II, Publish or Perish, Inc (1970).
 [14] See the supplementary material.
 [15] J. E. Moore and L. Balents, Phys. Rev. B **75**, 121306(R) (2007).
 [16] R. Roy, Phys. Rev. B **79**, 195322 (2009).
 [17] M. Oshikawa, Phys. Rev. B **50**, 17357 (1994).
 [18] Details for first-principles calculations can be found in [12].
 [19] H. Fukuyama, Prog. Theor. Phys. **45**, 704 (1971).
 [20] Due to the anisotropic dispersion, the scattering rate due to charge-neutral point scatterers shows momentum dependence even within the Born approximation. Explicitly,

$$\frac{1}{\tau_\lambda(\mathbf{k}, w)} = \pi n_i V_0^2 \frac{|\omega|^{3/2}}{2\pi^2 v^2 A^{1/2}} \left(1 + \frac{\lambda}{3} \text{sgn}(w) \frac{A k_1^2}{v^2 k_\perp^2 + A^2 k_1^4} \right) \quad (6)$$

where $\lambda = \pm$ indicates the positive/negative energy states. However, since the low temperature transport is dominated by the linear dispersion, we can neglect the momentum dependent part, which leads to the conventional structure of the scattering rate.

- [21] The T linear behavior of $\sigma_{11}(T)$ due to disorder scattering implies a vanishingly small conductivity in $T \rightarrow 0$ limit. This is an artifact of the simple (non self-consistent) Born approximation. Once the self-consistency is carefully considered, $\sigma_{11}(T)$ should approach a constant value as $T \rightarrow 0$.

SUPPLEMENTARY MATERIAL

1. A curve in 3D and its curvature and torsion

In this section, we describe the relation between the shape of a curve in 3D space and its curvature and torsion. Here we basically follow the contents in Ref. 13. A convenient way to describe a curve $C = C(t) = (x(t), y(t), z(t))$ is to use an orthogonal coordinate system $(\mathbf{t}, \mathbf{n}, \mathbf{b})$ where \mathbf{t} , \mathbf{n} , \mathbf{b} are the tangential, normal, and binormal vectors, respectively. To define \mathbf{t} , \mathbf{n} , \mathbf{b} we first consider the arclength, which is defined as

$$s(t) = \int_0^t dt' \left| \frac{dC(t')}{dt'} \right|. \quad (7)$$

For the following discussion, we reparametrize the curve C using the arclength s , which makes C to be a function of s , i.e., $C = C(s)$. Then \mathbf{t} , \mathbf{n} , \mathbf{b} are given by

$$\mathbf{t} \equiv \frac{dC}{ds}, \quad \mathbf{n} \equiv \frac{d^2C}{ds^2} / \left| \frac{d^2C}{ds^2} \right|, \quad \mathbf{b} \equiv \mathbf{t} \times \mathbf{n}, \quad (8)$$

and the curvature κ_C and torsion τ_C are defined as

$$\kappa_C(s) \equiv \left| \frac{d\mathbf{t}}{ds} \right|, \quad \frac{d\mathbf{b}}{ds} \equiv -\tau_C(s)\mathbf{n}. \quad (9)$$

Therefore κ_C measures the rate at which the tangential vector changes and τ_C measures the rate at which the curve C deviates from being a planar curve lying on the (\mathbf{t}, \mathbf{n}) space. In the case of the torsion τ_C , it has a following equivalent expression,

$$\tau_C = \frac{1}{\kappa_C^2} \left\langle \frac{dC}{ds} \times \frac{d^2C}{ds^2}, \frac{d^3C}{ds^3} \right\rangle, \quad (10)$$

where $\langle A, B \rangle$ indicates the inner product of two vectors A and B .

The relation between the shape of a curve and its curvature and torsion can be understood by considering two dimensional projections of the curve on the planes in which two vectors among $\{\mathbf{t}, \mathbf{n}, \mathbf{b}\}$ are adopted as a basis. To represent an arbitrary curve $C(s)$ we can choose a coordinate which satisfies $C(0) = 0$, $\frac{dC}{ds}\big|_{s=0} = (1, 0, 0)$, and $\frac{d^2C}{ds^2}\big|_{s=0} = (0, \kappa_C, 0)$. Then from Eq. (10), we obtain $\frac{d^3C}{ds^3}\big|_{s=0} = (a_1, a_2, \kappa_C \tau_C)$ where $a_{1,2}$ are arbitrary numbers.

Now we consider the Taylor expansion of $C(s) = (x(s), y(s), z(s))$ at $s = 0$,

$$C(s) = C(0) + s \frac{dC}{ds} \Big|_0 + \frac{s^2}{2} \frac{d^2C}{ds^2} \Big|_0 + \frac{s^3}{6} \frac{d^3C}{ds^3} \Big|_0 + O(s^4), \quad (11)$$

which gives rise to

$$\begin{aligned} x(s) &= s + O(s^3), \\ y(s) &= \frac{\kappa_C}{2} s^2 + O(s^3), \\ z(s) &= \frac{\kappa_C \tau_C}{6} s^3 + O(s^4). \end{aligned} \quad (12)$$

From the leading order terms, the projections of the curve C are described by $y = \frac{\kappa_C}{2} x^2$, $z = \frac{\kappa_C \tau_C}{6} x^3$, and $z^2 = \frac{2}{9} \frac{\tau_C^2}{\kappa_C} y^3$, which are lying on (\mathbf{t}, \mathbf{n}) , (\mathbf{t}, \mathbf{b}) , and (\mathbf{n}, \mathbf{b}) planes, respectively. A typical example of a curve in 3D and its 2D projections are shown in Fig. 2. It is to be noted that the projections of the curve on (\mathbf{t}, \mathbf{b}) and (\mathbf{n}, \mathbf{b}) planes, shown in Fig. 2 (c) and (d), respectively, cannot form a closed curve under smooth variations of the curve. Since the shapes of these 2D projections remain the same as long as the torsion is nonzero at the origin, we obtain the zero torsion condition $\tau_C = 0$ to form a closed curve. On the other hand, when $\tau_C = 0$, the curve moves on the 2D space spanned by (\mathbf{t}, \mathbf{n}) . The trajectory of the curve on (\mathbf{t}, \mathbf{n}) plane shown in Fig. 2 (b) can make a closed loop as long as the curvature κ_C is finite.

2. Effective Hamiltonian for topological phase transition in BiTeI

Let us first consider a general Hamiltonian defined in momentum space $H(\mathbf{k}) = H(k_x, k_y, k_z)$. Then the combined symmetry operation TM , which is the combination of the time reversal (T) and mirror ($M : y \rightarrow -y$), imposes the following constraint to the $H(\mathbf{k})$,

$$\begin{aligned} (TM)H(k_x, k_y, k_z)(TM)^{-1} \\ = H^*(k_x, k_y, k_z) = H(-k_x, k_y, -k_z). \end{aligned} \quad (13)$$

Assuming that the band touching point exists at $\mathbf{k}_c = (0, k_{y,c}, \pi)$, we derive the low energy Hamiltonian considering small momentum deviation from the band touching point. Due to the TM symmetry, the effective 2×2 Hamiltonian $H_{2 \times 2}(\mathbf{q})$ with $\mathbf{q} = \mathbf{k} - \mathbf{k}_c$, satisfies the following constraint,

$$\begin{aligned} (TM)H_{2 \times 2}(q_x, q_y, q_z)(TM)^{-1} &= H_{2 \times 2}^*(q_x, q_y, q_z) \\ &= H_{2 \times 2}^*(k_x, k_y - k_{y,c}, k_z - \pi) \\ &= H_{2 \times 2}(-k_x, k_y - k_{y,c}, -k_z - \pi) \\ &= H_{2 \times 2}(-k_x, k_y - k_{y,c}, -k_z + \pi) \\ &= H_{2 \times 2}(-q_x, q_y, -q_z). \end{aligned} \quad (14)$$

Therefore

$$H_{2 \times 2}^*(q_x, q_y, q_z) = H_{2 \times 2}(-q_x, q_y, -q_z) \quad (15)$$

For the generic 2×2 Hamiltonian $H_{2 \times 2}(\mathbf{q})$ given by,

$$H_{2 \times 2}(\mathbf{q}) = f_1(\mathbf{q})\tau_1 + f_2(\mathbf{q})\tau_2 + f_3(\mathbf{q})\tau_3, \quad (16)$$

the constraint in Eq. (15) leads to the following constraints to $f_{1,2,3}(\mathbf{q})$,

$$\begin{aligned} f_{1,3}(-q_x, q_y, -q_z) &= f_{x,z}(q_x, q_y, q_z) \\ f_2(-q_x, q_y, -q_z) &= -f_y(q_x, q_y, q_z) \end{aligned} \quad (17)$$

which means that $f_{1,3}$ (f_2) are even (odd) under the simultaneous sign change of q_x and q_z . Now we expand $f_{1,2,3}$ near the band touching point at $\mathbf{q} = 0$ and $P = P_c$ in the powers of $q_{x,y,z}$ and $\Delta P = P - P_c$. Due to the symmetry constraint in Eq. (17), up to linear order in $q_{x,y,z}$ and $\Delta P = P - P_c$, $f_{1,2,3}$ are given by

$$\begin{aligned} f_1 &= N_1 \Delta P + M_{12} q_y \\ f_2 &= M_{21} q_x + M_{23} q_z \\ f_3 &= N_3 \Delta P + M_{32} q_y \end{aligned} \quad (18)$$

where $N_{1,3}$ and $M_{12,21,23,32}$ are constants. The Hamiltonian at the critical point $\Delta P = 0$ can be written as

$$H_{2 \times 2}(\mathbf{q}) = M_{12} q_y \tau_1 + (M_{21} q_x + M_{23} q_z) \tau_2 + M_{32} q_y \tau_3, \quad (19)$$

Since $\text{Det}M = 0$, M always has an eigenvector ξ_1 with zero eigenvalue. Explicitly, $\xi_1^t = \frac{1}{\sqrt{M_{21}^2 + M_{23}^2}}(-M_{23}, 0, M_{21})$ where the superscript t means the transpose of a vector.

Let us introduce $\xi_2^t = \frac{1}{\sqrt{M_{21}^2 + M_{23}^2}}(M_{21}, 0, M_{23})$ and $\xi_3^t = (0, 1, 0)$. Then $\xi_{1,2,3}$ constitute an orthogonal basis. Using this, we consider following linear transformation,

$$\begin{aligned} \begin{pmatrix} q_x \\ q_y \\ q_z \end{pmatrix} &\equiv (\xi_1, \xi_2, \xi_3) \begin{pmatrix} p_1 \\ p_2 \\ p_3 \end{pmatrix} \\ &= \begin{pmatrix} \frac{-M_{23}}{\sqrt{M_{21}^2 + M_{23}^2}} p_1 + \frac{M_{21}}{\sqrt{M_{21}^2 + M_{23}^2}} p_2 \\ p_3 \\ \frac{M_{21}}{\sqrt{M_{21}^2 + M_{23}^2}} p_1 + \frac{M_{23}}{\sqrt{M_{21}^2 + M_{23}^2}} p_2 \end{pmatrix} \end{aligned} \quad (20)$$

Applying the above linear transformation, the Hamiltonian is given by $H_{2 \times 2}(\mathbf{p}) = \sum_{i=1,2,3} f_i(\mathbf{p})\tau_i$ in which

$$\begin{aligned} f_1 &= N_1 \Delta P + M_{12} p_3, \\ f_2 &= \sqrt{M_{21}^2 + M_{23}^2} p_2, \\ f_3 &= N_3 \Delta P + M_{32} p_3. \end{aligned} \quad (21)$$

It is to be noticed that p_1 does not appear in the Hamiltonian due to the fact the ξ_1 is the eigenvector of M with zero eigenvalue.

To fully account for the phase transition, the terms quadratic in p_i are necessary. In terms of the rotated momentum \mathbf{p} , the symmetry constraint in Eq. (17) can be written as

$$H_{2 \times 2}^*(p_1, p_2, p_3) = H_{2 \times 2}(-p_1, -p_2, p_3). \quad (22)$$

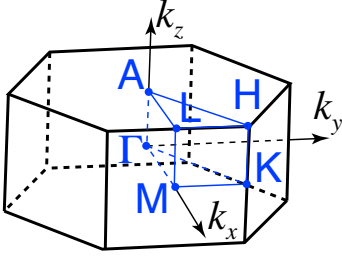


FIG. 4: (Color online) The hexagonal Brillouin zone of BiTeI.

Collecting terms satisfying the constraint above up to the quadratic order in p_i , $f_{1,2,3}$ can be written as

$$\begin{aligned} f_1 &= N_1 \Delta P + M_{12} p_3 + a_1 p_1^2 + a_2 p_2^2 + a_3 p_3^2 + a_4 p_1 p_2, \\ f_2 &= \sqrt{M_{21}^2 + M_{23}^2} p_2 + b_5 p_2 p_3 + b_6 p_3 p_1, \\ f_3 &= N_3 \Delta P + M_{32} p_3 + c_1 p_1^2 + c_2 p_2^2 + c_3 p_3^2 + c_4 p_1 p_2, \end{aligned} \quad (23)$$

where a_i, b_i, c_i ($i = 1, 2, \dots, 6$) are constants.

3. Topological phase transition in BiTeI

Recently, it is shown that when external pressure is applied to BiTeI, a direct phase transition from a normal insulator to a TI occurs mediated by accidental band touching points at the critical pressure $P = P_c$. The nature of the topological phase transition in BiTeI can be understood based on the general considerations developed in previous discussions. The key ingredient to understand the phase transition in this material is the fact that in the BZ shown in Fig. 4, the band touching occurs along the $A - H$ direction in $k_z = \pi$ plane, along which the Hamiltonian $H(\mathbf{k})$ is invariant under the combination of the time reversal (T) and mirror (M) symmetries. Picking one of the $A - H$ direction along the k_y axis, the combined symmetry operation TM imposes the following constraint to the Hamiltonian, $H^*(k_x, k_y, k_z) = H(-k_x, k_y, -k_z)$ because the mirror M changes k_y to $-k_y$. This symmetry constraint restricts the structure of the low energy Hamiltonian near the gap-closing points. Explicitly, the effective Hamiltonian near one of the band touching points can be written as $H(\mathbf{p}, \Delta P) = \sum_{i=1}^3 f_i(\mathbf{p}, \Delta P) \tau_i$ in which

$$\begin{aligned} f_1 &= N_1 \Delta P + M_{12} p_3 + a_1 p_1^2 + a_2 p_2^2 + a_3 p_3^2 + a_4 p_1 p_2, \\ f_2 &= \sqrt{M_{21}^2 + M_{23}^2} p_2 + b_5 p_2 p_3 + b_6 p_3 p_1, \\ f_3 &= N_3 \Delta P + M_{32} p_3 + c_1 p_1^2 + c_2 p_2^2 + c_3 p_3^2 + c_4 p_1 p_2, \end{aligned} \quad (24)$$

where a_i, b_i, c_i ($i = 1, 2, \dots, 6$) are constants and $\Delta P = P - P_c$. \mathbf{p} is the rotated momentum coordinates adapted to manifest the zero chirality of the band touching point. Therefore the terms linear in p_1 do not appear in $f_{1,2,3}$. The detailed

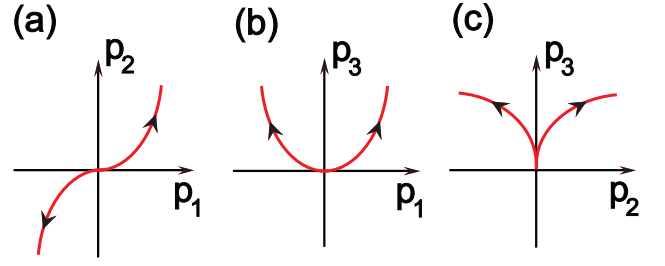


FIG. 5: (Color online) The 2D projections of the curve satisfying the gap-closing condition for the trajectory in Eq. (25) for $\alpha > 0, \beta > 0, \gamma > 0$.

procedures to derive the above Hamiltonian is shown in the Supplementary Material.

Let us first check the conditions to obtain a semi-metallic phase by finding the solution of $f_{1,2,3} = 0$. When $|\mathbf{p}| \ll 1$, $f_2 = 0$ leads to, $p_2 \propto p_3 p_1$. Inserting this result to the conditions $f_{1,2} = 0$, the general solution of the gapless point has the following structure, $p_1^* = \pm \alpha \sqrt{\Delta P}$, $p_2^* = \pm \beta (\Delta P)^{3/2}$, $p_3^* = \gamma \Delta P$ with α, β, γ constants. Here we assume that the gapless point exists only for $\Delta P > 0$. Therefore the trajectory of the gapless points is given by

$$\mathbf{p}^* = (\pm \alpha \sqrt{\Delta P}, \pm \beta (\Delta P)^{3/2}, \gamma \Delta P) \quad (25)$$

whose curvature and torsion at $\Delta P = 0$ is given by $\kappa_C = \frac{2\gamma}{\alpha^2}$ and $\tau_C = \frac{-3\beta}{\alpha\gamma}$, respectively. Since the curve has a finite torsion, we expect the trajectory of the gapless points would not form a closed loop under the smooth variation of the system, which is supported by the corresponding 2D projections of the curve shown in Fig. 5. Therefore once a semi-metallic phase occurs by splitting the band touching point at $\Delta P = 0$, the gapless point should persist for all ΔP , which is not consistent with the predictions of the first principle calculation.

The only way to describe the transition between two insulators is the occurrence of the direct transition between them via band touching at a single critical point. From the condition that the conduction band has a minimum, we have three equations of $\frac{\partial E_c(\mathbf{p})}{\partial p_i} = 0$ ($i = 1, 2, 3$). After careful examination of the three coupled equations, we have found that there is a unique solution given by

$$\mathbf{p}^{\min} = (0, 0, -\frac{N_1 M_{12} + N_3 M_{32}}{M_{12}^2 + M_{32}^2} \Delta P). \quad (26)$$

Therefore the direct transition between two gapped phases requires that the extrema of the valence and conduction bands move along a particular direction, the p_3 direction throughout the phase transition. Interestingly, the p_3 direction corresponds to the k_y direction of the original coordinate, which is nothing but one of the $A - H$ direction in the BZ. Because of the C_{3v} point group symmetry, the conduction (valence) band with the Rashba-type spin-orbit coupling develops a dispersion minimum (maximum) along the $A - H$ line for any $\Delta P \neq 0$. Moreover, since the $A - H$ line is on the $k_z = \pi$

plane satisfying the time-reversal invariance, the band touching can induce the topological phase transition. Explicitly, in the $k_z = \pi$ plane, the effective Hamiltonian near a gap-closing point can be written as a two dimensional massive Dirac Hamiltonian, in which ΔP plays the role of the mass term. Therefore a band touching point can change the Z_2 invariant on the $k_z = \pi$ plane by 1 through the sign change of ΔP . Since there are 3 pairs of band touching points on the same plane, the strong index ν_0 changes by 1 reflecting the emergence of the TI through the band touching.

The Hessian matrix $\hat{H}_{ij}^{\min} = \frac{\partial^2 E_c}{\partial p_i \partial p_j}$ has a block diagonal form with $\hat{H}_{13}^{\min} = \hat{H}_{23}^{\min} = 0$ at $\mathbf{p} = \mathbf{p}^{\min}$. The other nonzero components of \hat{H}^{\min} satisfies

$$\hat{H}_{33}^{\min} > 0, \quad \text{Det} \begin{pmatrix} H_{11}^{\min} & H_{12}^{\min} \\ H_{21}^{\min} & H_{22}^{\min} \end{pmatrix} = C' \Delta P,$$

where C' is a constant. Therefore the conduction band always has a minimum along the p_3 direction. On the other hand, the determinant of the Hessian matrix for the p_1, p_2 directions, normal to the $A-H$ line, shows sign change across the phase transition, which predicts the appearance of a saddle point in (p_1, p_2) plane for one of the gapped phase. Since the normal insulator for $\Delta P < 0$ possesses the conventional dispersion minimum or maximum, we can set $C' < 0$. Therefore the TI should possess saddle points in energy dispersion. The change of the band dispersion across the topological phase transition is explicitly shown in Fig. 3 from the band structure obtained by first principle calculation.

4. Perturbative renormalization group approach to the quantum critical point

The Hamiltonian for the anisotropic QCP can be written as

$$H = -iv\partial_1\tau_1 - iv\partial_2\tau_2 - A\partial_3^2\tau_3, \quad (27)$$

Compared to the Hamiltonian in the main text, the coordinates x_1 and x_3 are interchanged for convenience. In the main text, we have considered the following scale transformations,

$$t = b\tilde{t}, \quad x_{1,2} = b\tilde{x}_{1,2}, \quad x_3 = b^{1/2}\tilde{x}_3, \quad (28)$$

which lead to the conclusion that both the point disorder and $1/r$ Coulomb potential are irrelevant perturbation in tree level analysis. Here we consider a more general scale transformation without specifying the scaling dimension of x_3 and t . Namely,

$$t = b^z\tilde{t}, \quad x_{1,2} = b\tilde{x}_{1,2}, \quad x_3 = b^{z_3}\tilde{x}_3. \quad (29)$$

The effective action for free electrons at QCP can be written as

$$S_0 = \int dtd^3x [\psi^\dagger (i\partial_t + iv\partial_1\tau_1 + iv\partial_2\tau_2 + A\partial_3^2\tau_3)\psi]. \quad (30)$$

The invariance of S_0 under the scale transformation in Eq. (29) leads to the following scaling relations at tree level,

$$\tilde{\psi}(\mathbf{x}, t) = b^{1+\frac{z_3}{2}}\psi(\mathbf{x}, t), \quad \tilde{v} = b^{z-1}v, \quad \tilde{A} = b^{z-2z_3}A. \quad (31)$$

If we assume that the velocity v is a marginal coupling at tree level, we obtain $z = 1$. In this case, from the scale transformation of A , we can impose $z - 2z_3 \leq 0$, which leads to $z_3 \geq 1/2$. On the other hand, if we assume that A is a marginal coupling, we obtain $z = 2z_3$. From the scaling dimension of v , i.e., $z - 1 = 2z_3 - 1 \leq 0$, we obtain $z_3 < 1/2$. Therefore z and z_3 should satisfy either $z = 1$ and $z_3 \geq 1/2$ or $z = 2z_3$ and $0 < z_3 < 1/2$.

Under this scale transformation, the disorder potential for the short-ranged random disorder Δ_{ij} transforms as $\tilde{\Delta}_{ij} = b^{2z-2-z_3}\Delta_{ij}$, in which the scaling dimension satisfies $2z - 2 - z_3 < -1/2$. Namely, the disorder is always irrelevant. Therefore in the following we neglect the disorder effect and focus on the influence of $1/r$ Coulomb potential to the Gaussian fixed point.

To perform the scaling analysis and one-loop renormalization group calculation, it is convenient to write the effective action in the momentum space, which is given by

$$S = S_0 + S_C, \quad (32)$$

in which

$$S_0 = \frac{V}{(2\pi)^3} \int dtd^3k \psi^\dagger [i\partial_t - v(k_1\tau_1 + k_2\tau_2) - Ak_3^2\tau_3]\psi, \\ S_C = \frac{g^2}{2} \frac{V^2}{(2\pi)^9} \int dtd^3q d^3k_1 d^3k_2 \frac{1}{q_\perp^2 + q_3^2} \\ \times \psi^\dagger(\mathbf{k}_1 + \mathbf{q}, t) \psi(\mathbf{k}_1, t) \psi^\dagger(\mathbf{k}_2, t) \psi(\mathbf{k}_2 + \mathbf{q}, t), \quad (33)$$

where $g^2 = e^2/\varepsilon$ and $q_\perp^2 = q_1^2 + q_2^2$.

Under the scale transformation

$$\tilde{k}_{1,2} = bk_{1,2}, \quad \tilde{k}_3 = b^{z_3}k_3, \quad \tilde{t} = \frac{1}{b^z}t, \quad (34)$$

the Coulomb interaction $V(q) = g^2/(q_\perp^2 + q_3^2)$ transforms as

$$V(\tilde{q}) = \frac{g^2}{\frac{1}{b^2}\tilde{q}_\perp^2 + \frac{1}{b^{2z_3}}\tilde{q}_3^2} \rightarrow \begin{cases} \frac{b^2g^2}{\tilde{q}_\perp^2} & \text{if } z_3 > 1, \\ \frac{b^2g^2}{\tilde{q}_\perp^2 + \tilde{q}_3^2} & \text{if } z_3 = 1, \\ \frac{b^{2z_3}g^2}{\tilde{q}_3^2} & \text{if } z_3 < 1, \end{cases}$$

where we display the asymptotic form of the Coulomb interaction in the low energy limit. The resulting scaling relation of g^2 is

$$\tilde{g}^2 = \begin{cases} g^2 b^{z-z_3} & \text{if } z_3 > 1, \\ g^2 & \text{if } z_3 = 1, \\ g^2 b^{z+z_3-2} & \text{if } z_3 < 1. \end{cases}$$

Taking into account of the scaling analysis of S_0 and the relations of z_3 and z discussed previously, we can see that g^2 is always irrelevant except when $z = z_3 = 1$ where g^2 is marginal.

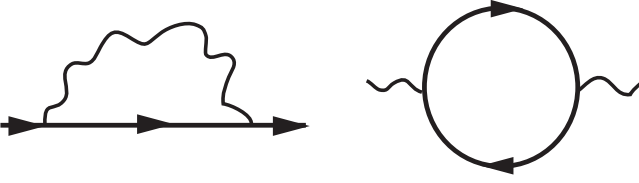


FIG. 6: (Color online) One-loop diagrams that determine the flow of the coupling constants. (Left) electron self energy. (Right) photon self energy.

Therefore in the following we perform a one-loop perturbative renormalization group analysis to confirm the relevance or irrelevant of the marginal coupling g^2 when $z = z_3 = 1$.

To perform the renormalization group analysis we first introduce a bosonic Hubbard-Stratonovich field φ to treat the instantaneous Coulomb interaction. Then the Euclidean effective action describing the low energy electrons coupled to long range Coulomb interaction can be written as

$$S_{\text{bare}} = \int d^4x \left[\bar{\psi} \{ \gamma_0 (\partial_0 + ig\varphi) + v(\gamma_1 \partial_1 + \gamma_2 \partial_2) - A \partial_3^2 \} \psi + \frac{1}{2} (\partial_i \varphi)^2 \right], \quad (35)$$

where the matrices $\gamma_{0,1,2}$, satisfying $\{\gamma_i, \gamma_j\} = 2\delta_{ij}$, are defined as $\gamma_0 = \tau_3, \gamma_1 = \tau_2, \gamma_2 = -\tau_1$. ψ (φ) represents an electron (photon) field operator and $\bar{\psi} = \psi^\dagger \gamma_0$. The non-interacting electron and photon Green's functions are given by

$$G_0(k_0, \mathbf{k}) = \frac{-i[\gamma_0 k_0 + v(\gamma_1 k_1 + \gamma_2 k_2)] + A k_3^2}{k_0^2 + v^2 k_\perp^2 + A^2 k_3^4},$$

$$D_0(k_0, \mathbf{k}) = \frac{1}{k_\perp^2 + \eta k_3^2}, \quad (36)$$

where $k_\perp^2 = k_1^2 + k_2^2$. Here we introduce η describing the anisotropy of the photon propagators, which is induced by the anisotropy of the electron dispersion. ($\eta = 1$ if there is no coupling between the electron and photon.) We perform a one-loop Kadanoff-Wilson RG analysis of S_{bare} . We trace out high energy modes in the energy range of $[Ee^{-\ell}, E]$ considering constant energy surfaces and obtain a renormalized action. Because of the anisotropic dispersion, we have introduced two momentum cutoffs Λ_\perp and Λ_3 .

Let us first consider the renormalization of v and A by computing the electron self-energy $\Sigma(k)$. At one-loop order, $\Sigma(k)$ can be written as

$$\begin{aligned} \Sigma(k_0, \mathbf{k}_\perp, k_3) &= -g^2 \int_{-\infty}^{\infty} \frac{dq_0}{2\pi} \int' \frac{d^3q}{(2\pi)^3} \gamma_0 G_0(q) \gamma_0 D_0(k-q) \\ &= -\frac{g^2}{2} \int' \frac{d^3q}{(2\pi)^3} \frac{[iv(\gamma_1 q_1 + \gamma_2 q_2) + A q_3^2]}{\sqrt{v^2 q_\perp^2 + A^2 q_3^4}} \\ &\quad \times \frac{1}{[(\mathbf{k}_\perp - \mathbf{q}_\perp)^2 + \eta(k_3 - q_3)^2]}, \end{aligned} \quad (37)$$

where $\int' \frac{d^3q}{(2\pi)^3}$ indicates the integration over the large momentum lying within the high energy shell. For convenience, we define a dimensionless quantity $\bar{A} \equiv \frac{A\Lambda_3}{v}$. Then $\Sigma(k)$ can be written as

$$\begin{aligned} \Sigma(k) &= -iv(\gamma_1 k_1 + \gamma_2 k_2) \ell I_1(\alpha, \bar{A}, \eta) - v \bar{A}^2 \Lambda_3 \ell I_2(\alpha, \bar{A}, \eta) \\ &\quad - \frac{v \bar{A}}{\Lambda_3} k_3^2 \ell I_3(\alpha, \bar{A}, \eta) \end{aligned} \quad (38)$$

where $\ell = \ln b$ is the usual RG parameter. $I_1(\alpha, \bar{A}, \eta)$ ($I_3(\alpha, \bar{A}, \eta)$) describes the renormalization of v (\bar{A}). $I_2(\alpha, \bar{A}, \eta)$ merely describes the shift of the critical pressure that is required to tune the system to the quantum critical point. Explicitly $I_{1,2,3}(\alpha, \bar{A}, \eta)$ are given by

$$\begin{aligned} I_1(\alpha, \bar{A}, \eta) &= \frac{\alpha}{\pi} \bar{A}^3 \int_0^1 dx \frac{1-x^4}{(\eta x^2 - \bar{A}^2 x^4 + \bar{A}^2)^2}, \\ I_2(\alpha, \bar{A}, \eta) &= \frac{\alpha}{\pi} \frac{1}{\eta} \int_0^1 dx \frac{x^2}{(x^2 - \frac{\bar{A}^2}{\eta} x^4 + \frac{\bar{A}^2}{\eta})}, \\ I_3(\alpha, \bar{A}, \eta) &= \frac{\alpha}{\pi} \bar{A} \int_0^1 dx \frac{(3x^4 \eta^2 + \bar{A}^2 x^6 \eta - x^2 \bar{A}^2 \eta)}{(\eta x^2 - \bar{A}^2 x^4 + \bar{A}^2)^3}, \end{aligned} \quad (39)$$

where the fine structure constant $\alpha \equiv \frac{g^2}{4\pi v}$.

Next we compute the one-loop photon self-energy $\Pi(k)$, which is given by

$$\Pi(k) = g^2 \int_{-\infty}^{\infty} \frac{dq_0}{2\pi} \int' \frac{d^3q}{(2\pi)^3} \text{Tr}[\gamma_0 G_0(q) \gamma_0 G_0(k+q)], \quad (40)$$

To determine the renormalization of the bare photon propagator $D_0(k)$ by $\Pi(k)$, we expand $\Pi(k)$ in powers of k_i up to quadratic order, which leads to

$$\Pi(k) = -k_\perp^2 \ell I_4(\alpha, \bar{A}, \eta) - k_3^2 \ell I_5(\alpha, \bar{A}, \eta), \quad (41)$$

in which

$$I_4(\alpha, \bar{A}, \eta) = \frac{3}{10\pi} \frac{\alpha}{\bar{A}}, \quad I_5(\alpha, \bar{A}, \eta) = \frac{8}{21\pi} \alpha \bar{A}, \quad (42)$$

Including $\Sigma(k)$ and $\Pi(k)$, the full effective action can be written as

$$S_{\text{renorm}} = S_{\text{bare}} + \int d^4x \bar{\psi} (-\Sigma) \psi + \int d^4x \frac{1}{2} \varphi (-\Pi) \varphi, \quad (43)$$

The one loop RG equations can be obtained in the following way. At first, we rescale the space-time coordinates,

$$x_0 = \tilde{x}_0 b^z, \quad x_1 = \tilde{x}_1 b, \quad x_2 = \tilde{x}_2 b, \quad x_3 = \tilde{x}_3 b^{z_3}, \quad (44)$$

where the tilde is used to indicate the scaled variable. Then we introduce renormalization constants $Z_\psi, Z_\varphi, Z_g, Z_v, Z_{\bar{A}}$,

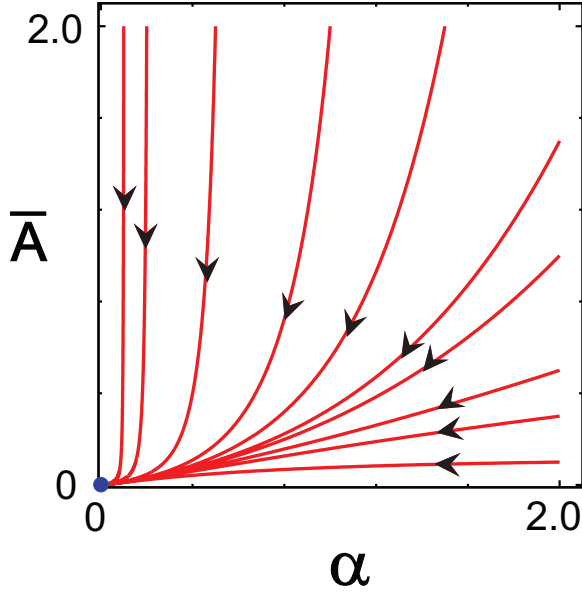


FIG. 7: (Color online) The RG flow for $z_3 = 1$ in (α, \bar{A}) space. There is only one fixed point at the origin. Both α and \bar{A} exponentially decrease to zero.

and Z_η in the following way, $\psi = Z_\psi^{-1/2} \tilde{\psi}$, $\varphi = Z_\varphi^{-1/2} \tilde{\varphi}$, $g = Z_g^{-1/2} \tilde{g}$, $v = Z_v^{-1} \tilde{v}$, $\bar{A} = Z_{\bar{A}}^{-1} \tilde{\bar{A}}$, $\eta = Z_\eta^{-1} \tilde{\eta}$. Then we assume that the renormalized action S_{renorm} has the same form as the bare action S_{bare} , which leads to

$$\begin{aligned} \frac{d \ln v}{d\ell} &= z - 1 + I_1(\alpha, \bar{A}, \eta), \\ \frac{d \ln \bar{A}}{d\ell} &= z - 2z_3 + I_3(\alpha, \bar{A}, \eta), \\ \frac{d \ln g^2}{d\ell} &= z - z_3 - I_4(\alpha, \bar{A}, \eta), \\ \frac{d \ln \eta}{d\ell} &= 2 - 2z_3 - I_4(\alpha, \bar{A}, \eta) + \frac{1}{\eta} I_5(\alpha, \bar{A}, \eta), \end{aligned} \quad (45)$$

or, in terms of dimensionless variables $\alpha \equiv \frac{g^2}{4\pi v}$ and $\bar{A} \equiv \frac{A\Lambda_3}{v}$, the RG equations are

$$\begin{aligned} \frac{d \ln \alpha}{d\ell} &= 1 - z_3 - I_1(\alpha, \bar{A}, \eta) - I_4(\alpha, \bar{A}, \eta), \\ \frac{d \ln \bar{A}}{d\ell} &= 1 - 2z_3 + I_3(\alpha, \bar{A}, \eta) - I_1(\alpha, \bar{A}, \eta), \\ \frac{d \ln \eta}{d\ell} &= 2 - 2z_3 - I_4(\alpha, \bar{A}, \eta) + \frac{1}{\eta} I_5(\alpha, \bar{A}, \eta). \end{aligned} \quad (46)$$

Now let us describe the RG flow for $z_3 = 1$ case in which the fine structure constant α is marginal. It is interesting to note that the RG equations for α consists of two parts, I_1 from the velocity renormalization and I_4 from the dielectric constant renormalization. (Note that since the charge e is protected from perturbative renormalization due to gauge invariance, the renormalization of the coupling constant $g^2 = e^2/\varepsilon$ results from the dielectric constant renormalization.) Since

$I_1 \approx \alpha/4$ for small \bar{A} , the RG equation for α is given by

$$\frac{d \ln \alpha}{d\ell} = -\frac{\alpha}{4} - \frac{3}{10\pi} \frac{\alpha}{\bar{A}}, \quad (47)$$

which shows that the velocity renormalization (the first term in Eq. (47)) leads to the logarithmic decrement of α . However, due to the exponential decrement of \bar{A} (it is an irrelevant variable), the dielectric constant renormalization (the second term in Eq. (47)) dominates the RG flow of α in the small \bar{A} limit, which changes the logarithmic decrement of α to the exponential decrement in the low energy limit. *Namely, the irrelevant variable \bar{A} plays the role of a dangerously irrelevant variable.* In the end, the coupling constant α , which was marginal at tree level, turns into an irrelevant variable under the one-loop renormalization group correction.

The singular $1/\bar{A}$ behavior of the dielectric constant renormalization I_4 can be understood in the following way. When $\bar{A} = 0$, the photon self-energy is given by

$$\Pi(k) = -\frac{g^2}{8v} k_\perp^2 \int' \frac{d^3 q}{(2\pi)^3} \frac{1}{q_\perp^3}, \quad (48)$$

Since the integrand is independent of q_3 momentum, the energy shell integral simply becomes

$$\int' d^3 q = \int_{-\Lambda_3}^{\Lambda_3} dq_3 \int' d^2 q_\perp = 2\Lambda_3 \int_{\Lambda_\perp e^{-\ell}}^{\Lambda_\perp} 2\pi q_\perp dq_\perp, \quad (49)$$

which leads to

$$\Pi(k) = -\frac{g^2}{16\pi^2 v} k_\perp^2 \left(\frac{\Lambda_3}{\Lambda_\perp} \right) \ell = -\frac{g^2}{16\pi^2 v} k_\perp^2 \left(\frac{1}{\bar{A}} \right) \ell, \quad (50)$$

In the case of the isotropic system such as the 3D Dirac system, $\frac{\Lambda_3}{\Lambda_\perp} = 1$, which leads to the usual logarithmic renormalization of $\Pi(k)$. However, in the present system, due to the strong anisotropy of the electron dispersion, $\frac{\Lambda_3}{\Lambda_\perp} = \frac{1}{\bar{A}}$ becomes strongly enhanced in the low energy limit, which is the origin of the singular enhancement of the dielectric constant renormalization.

The RG flow near the fixed point for $z_3 = 1$

Since \bar{A} is an irrelevant variable, it will become very small near the fixed point. When $\bar{A} \ll 1$, the RG equations are given by

$$\begin{aligned} \frac{d \ln \alpha}{d\ell} &= -\frac{\alpha}{4\sqrt{\eta}} - \frac{3}{10\pi} \frac{\alpha}{\bar{A}}, \\ \frac{d \ln \bar{A}}{d\ell} &= -1, \\ \frac{d \ln \eta}{d\ell} &= -\frac{3}{10\pi} \frac{\alpha}{\bar{A}} + \frac{8}{21\pi} \frac{\alpha \bar{A}}{\eta}. \end{aligned} \quad (51)$$

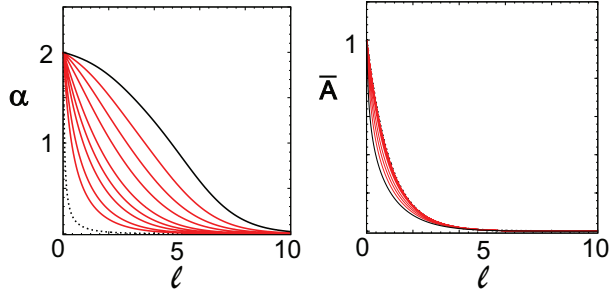


FIG. 8: (Color online) The flow of $\alpha(\bar{A})$ varying the initial values of \bar{A} (α) when $z_3 = 1$. (Left) For a fixed initial values of $\alpha = 2$, the initial values of \bar{A} varies from 0.01 (dotted lines), 0.1, 0.2, 0.5, 1.0, 2.0, 5.0, 10.0, 20.0, 50.0 (black solid line). (Right) For a fixed initial values of $\bar{A} = 1$, the initial values of α varies from 0.01 (dotted lines), 0.1, 0.2, 0.5, 1.0, 2.0, 5.0, 10.0, 20.0, 50.0 (black solid line).

For $\bar{A} = \bar{A}(0)e^{-\ell}$,

$$\begin{aligned} \frac{d \ln \alpha}{d \ell} &\approx -\frac{3}{10\pi} \frac{\alpha}{\bar{A}}, \\ \frac{d \ln \eta}{d \ell} &\approx -\frac{3}{10\pi} \frac{\alpha}{\bar{A}}, \end{aligned} \quad (52)$$

which leads to

$$\begin{aligned} \alpha(\ell) &= \frac{\alpha(0)}{1 + \frac{3}{10\pi} \frac{\alpha(0)}{\bar{A}(0)} (e^\ell - 1)}, \\ \bar{A}(\ell) &= \bar{A}(0)e^{-\ell}, \\ \eta(\ell) &= \eta(0)e^{-\ell}, \end{aligned} \quad (53)$$

The exponential decrement of η means that the effective Coulomb interaction becomes $V(\mathbf{q}) \approx \frac{1}{q_\perp^2}$ in the end.

The RG equations for v and A (dimensionfull variables) are given by

$$\begin{aligned} \frac{d \ln v}{d \ell} &= z - 1 + I_1(\alpha, \bar{A}, \eta), \\ \frac{d \ln A}{d \ell} &= z - 2 + I_3(\alpha, \bar{A}, \eta), \end{aligned} \quad (54)$$

Notice that the flow equations for v and A depend on the dynamical exponent z . In the low energy limit where $z \approx 1$, the RG equations become

$$\begin{aligned} \frac{d \ln v}{d \ell} &= I_1(\alpha, \bar{A}, \eta) = \frac{\alpha}{4} \approx \text{const} \times e^{-\ell}, \\ \frac{d \ln A}{d \ell} &= -1, \end{aligned} \quad (55)$$

which lead to

$$v(\ell) = v(0)e^{-\text{const} \times e^{-\ell}} \rightarrow v(0), \quad A(\ell) = A(0)e^{-\ell}. \quad (56)$$

Interestingly, the velocity saturates to a constant value while A decreases exponentially.